van der Waals–stabilized Rydberg aggregates

H. Zoubi,* A. Eisfeld, and S. Wüster
Max Planck Institute for the Physics of Complex Systems, Nöthnitzer Strasse 38, 01187 Dresden, Germany
(Received 20 December 2013; revised manuscript received 14 May 2014; published 29 May 2014)

Assemblies of Rydberg atoms subject to resonant dipole-dipole interactions exhibit Frenkel excitons. We show that van der Waals shifts can significantly modify the exciton wave function, whenever atoms approach each other closely. As a result, attractive dipole-dipole potentials and repulsive van der Waals interactions can be combined to form stable one-dimensional atom chains, akin to bound aggregates. Here the van der Waals shifts ensure a stronger homogeneous delocalization of a single excitation over the whole chain, enabling it to bind several atoms. When brought into unstable configurations, such Rydberg aggregates allow the direct monitoring of their dissociation dynamics.

DOI: 10.1103/PhysRevA.89.053426 PACS number(s): 32.80.Ee, 37.10.Jk, 71.35.−y

I. INTRODUCTION

van der Waals (vdW) forces between ground-state molecules or atoms can lead to the formation of molecular crystals and noble atom solids, without the need for electron sharing between the individual constituents. Optical and electrical properties in these aggregates are dominated by resonant interactions of transition dipoles which lead to the appearance of Frenkel excitons [1,2], in which an electronic excitation can be delocalized in the lattice. Nonresonant interactions of vdW type lead to a change of the transition energies, since they affect the excited state differently than the ground state. This energy shift is homogeneous (i.e., the same for all monomers) for bulk crystals [3–5] and in this context is termed the gas to crystal shift. For small structures of molecules, e.g., oligomers [6] or finite-size domains on surfaces [7,8], the shift is not homogeneous any more.

Here we show that this inhomogeneity of the vdW shifts can strongly influence the entire exciton wave function. To this end we consider assemblies of Rydberg atoms, which have huge transition dipoles (connecting two highly excited states) and hence can support Frenkel excitons over large distances [9,10]. Under conditions of one-dimensional confinement we further demonstrate the possibility of stable chains of Rydberg atoms, which form Rydberg "aggregates" similar to the molecular situation [4]. The stable chain is formed by a competition between attractive forces generated by resonant dipole-dipole interactions and repulsive vdW interactions. This bears some similarities to excimers. For short chains (e.g., trimers) prepared in unstable configurations, we find an interesting breakup dynamics, reminiscent of molecular dissociation. Due to the exaggerated properties of Rydberg atoms, the dissociation can be directly monitored in real space.

The basic effect of the inhomogeneous vdW shifts can be understood by the following simple consideration. For comparatively large distances between Rydberg atoms in a chain, resonant dipole-dipole processes of the type $ns + np \leftrightarrow np + ns$ are dominant [11,12] and support collective exciton states [9,10,13] which can have repulsive or attractive character [10]. If the distances between Rydberg atoms in a chain become shorter, off-resonant contributions to the system's electronic energies increase and can be modeled by the addition of vdW potentials. This can give rise to on-site excitation energy shifts that depend on the geometry of the atomic assembly. For a trimer, for example, this effect can shift the central site out of resonance, since it has a different local environment than the outer sites. In *attractive exciton states*, i.e., those that result in attractive dipole-dipole interactions, with repulsive vdW potentials, the site energy shifts near the chain center cause a stronger delocalization of the excitation towards the chain edges. This results in much more homogeneous attraction throughout the chain, allowing the stabilization of attractive exciton states [10] by vdW repulsion. One-dimensional Rydberg chains can then essentially form bound states with many atoms, resembling the vdW bound self-assembled molecular aggregates or molecular crystals. Previous work focused on two and three Rydberg atoms, which can form bound molecular states in three dimensions [14–17].

For light alkali-metal atoms, atomic motion in the potentials discussed here can become relevant on the time scale of Rydberg state lifetimes [18], resulting in flexible Rydberg aggregates [10,19–21]. With "flexible" we imply that the atoms are free to move and their motion is relevant, in contrast to a frozen-gas approximation. We investigate the behavior of such a flexible Rydberg trimer and find that it may exhibit interesting dissociation dynamics that can be monitored in time and space due to the detailed control afforded by ultracold Rydberg physics.

This paper is organized as follows. In Sec. II we discuss exciton states of a static linear aggregate. The atomic motion in dynamic linear aggregates is discussed in Sec. III. A summary is given in Sec. IV. Analytical solutions for a symmetric aggregate are presented in the Appendix.

II. STATIC RYDBERG AGGREGATE

We first analyze a frozen one-dimensional linear Rydberg aggregate, in which the positions $R_1, \ldots, R_N \equiv \boldsymbol{R}$ of the atoms are assumed fixed, and treat the electronic excited states of the system, where we use a simple model of N two-level Rydberg atoms [see Fig. 1(a)]. We define atomic states $|nl\rangle$, with principal quantum number n and angular momentum l, and concentrate on a lower Rydberg state, $|s_i\rangle = |ns\rangle$,

*zoubi@pks.mpg.de

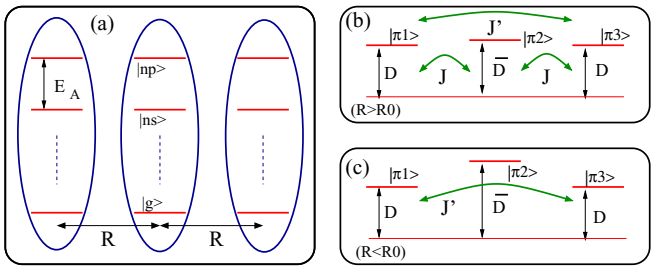

FIG. 1. (Color online) (a) Single-body states of three Rydberg atoms are illustrated schematically. We show the $|ns\rangle$ and $|np\rangle$ states, with the transition energy $E_A = E_p - E_s$, and the absolute ground state $|g\rangle$. (b) The states $|\pi_i\rangle$, with $(i = 1,2,3)$, are presented. For large interatomic distance relative to the crossover distance, $R > R_0$, the three $|\pi_i\rangle$ states are close to resonance, $D \approx \bar{D}$, and energy transfer is permitted among them with transfer parameters J and J'. (c) For a small interatomic distance, $R_0 > R$, the states $|\pi_1\rangle$ and $|\pi_3\rangle$ have the same vdW shift of D, but $|\pi_2\rangle$ experiences a different shift $\bar{D}$, with $\bar{D} \gg D$. Hence, the $|\pi_2\rangle$ state is no longer resonant with $|\pi_{1,3}\rangle$. Now energy transfer is allowed only among the $|\pi_1\rangle$ and $|\pi_3\rangle$ states with the transfer parameter J'.

of energy E_s and a higher Rydberg state, $|p_i\rangle = |np\rangle$, of energy E_p. Here the index $i = 1,\ldots,N$ labels the atoms. We consider the dynamics in the subspace spanned by the states $|\pi_i\rangle = |s_1,\ldots,s_{i-1},p_i,s_{i+1}\ldots,s_N\rangle$, where only the ith atom is in the (np) state and all others are in the (ns) state. In this subspace we write the relevant effective Hamiltonian as

$$H_{\rm ex} = \sum_i E_i(\boldsymbol{R})|\pi_i\rangle\langle\pi_i| + \sum_{ij} J_{ij}(\boldsymbol{R})|\pi_i\rangle\langle\pi_j|, \qquad (1)$$

where $J_{ij}(R_i,R_j) \propto 1/|R_i - R_j|^3$ is the resonant dipole-dipole interaction. It is responsible for transfer of excitation between states $|\pi_i\rangle$ and $|\pi_j\rangle$. The diagonal energies E_i contain the off-resonant vdW interactions. They can approximately be written as $E_i = E_0 + E_i^{(\rm vdW)}(\mathbf{R})$, with $E_0 = E_p + (N-1)E_s$, and

$$E_i^{(\rm vdW)}(\mathbf{R}) \approx \sum_{\ell\neq i} \frac{hC_6^{sp}}{R_{i\ell}^6} + \frac{1}{2}\sum_{j\neq i}\sum_{\ell\neq i,j} \frac{hC_6^{ss}}{R_{j\ell}^6}, \qquad (2)$$

where $R_{i\ell} = |R_i - R_\ell|$ and h is the Planck constant. Here C_6^{ss} and C_6^{sp} denote the C_6 coefficients for the vdW interaction between two atoms in the s state and between one atom in the s state and the other in the p state, respectively. With Eq. (1) we employ an effective model that encapsulates the essential features that would arise from a more complicated Hamiltonian taking into account all electronic states per atom. The use of binary C_6 coefficients is usually a good approximation and makes the results particularly transparent. For a discussion of three-body effects, see Ref. [22].

Note that the magnitude and the sign of the C_6 coefficients depend on the chosen states (and atomic species). We will come back to this point below. The resonant interaction J_{ij} depends on the magnetic quantum number [9,23,24] which leads to an anisotropic spatial interaction. For the following considerations (where we restrict ourselves to one-dimensional geometries, i.e., the atoms form a one-dimensional chain) we ignore this anisotropy and write

$$J_{ij}(R_i,R_j) = \frac{hC_3}{|R_{ij}|^3}, \qquad (3)$$

where C_3 can be both positive or negative. How this can be achieved is discussed, e.g., in Refs. [20,21,22].

Diagonalization of the Hamiltonian (1) for fixed positions $\boldsymbol{R}$ leads to (adiabatic) eigenstates

$$|\psi_k(\boldsymbol{R})\rangle = \sum_{i=1}^{N} c_k^i(\boldsymbol{R})|\pi_i\rangle \qquad (4)$$

and eigenenergies $U_k(\boldsymbol{R})$. To illustrate the basic electronic structure, we discuss the case of a finite linear chain of three Rydberg atoms with equal spacing R between nearest neighbors. The above excitonic Hamiltonian (1) can then be written in the basis $\{|\pi_1\rangle,|\pi_2\rangle,|\pi_3\rangle\}$ as

$$H_{\rm ex} = E_0 + \begin{pmatrix} D & J & J' \\ J & \bar{D} & J \\ J' & J & D \end{pmatrix}, \qquad (5)$$

where $J = \frac{hC_3}{R^3}$ and $J' = J/8$, with

$$D = \frac{h\left(C_6^{sp} + C_6^{ss}\right)}{R^6} + D', \quad \bar{D} = \frac{2hC_6^{sp}}{R^6} + \bar{D}', \qquad (6)$$

where $D' = hC_6^{sp}/(64R^6)$ and $\bar{D}' = hC_6^{ss}/(64R^6)$. Note that D', $\bar{D}'$, and J' are small and can often be neglected to a good approximation.

From Hamiltonian (5) it is apparent that the relevance of the relative shift $(\bar{D} - D)$ in the site energy of atom 2 is determined by the ratio of $J \sim R^{-3}$ and $(\bar{D} - D) \sim R^{-6}$, which depend differently on the distance between the atoms. In particular we consider two cases: large and small interatomic distances relative to the "crossover distance," $R_0 \sim |(C_6^{sp} - C_6^{ss})/C_3|^{1/3}$, where the magnitude of J becomes of the order of $(\bar{D} - D)$. For $R > R_0$ the three states $|\pi_i\rangle$ with $(i = 1,2,3)$ are close to resonance and energy transfer is possible among them, as presented in Fig. 1(b). Hence the three states can be coherently mixed to form excitonic states. In the case of $R < R_0$ the two states $|\pi_1\rangle$ and $|\pi_3\rangle$ are in resonance but the state $|\pi_2\rangle$ is shifted off resonance due to vdW interactions, as illustrated in Fig. 1(c). Now energy transfer is possible mainly among the states $|\pi_1\rangle$ and $|\pi_3\rangle$, which combine into excitonic states, while the state $|\pi_2\rangle$ remains a localized state. Thus, in this case the small J' cannot be neglected.

This can also clearly be seen in our numerical calculations. For these we choose parameters $C_3 = -1.16$ GHz/μm^3; $C_6^{ss} = 47$ MHz/μm^6, appropriate for a principal quantum number $n = 30$ of Li [25]; and $C_6^{sp} \approx +282$ MHz/μm^6. The latter might require external modification of interaction strengths with the use of Förster resonances [26,27]. The use of a Förster resonance would also allow independently controlling the sign of C_6^{sp} and that of C_3.

In Fig. 2(a) we plot $U_k(R)$, for the three collective potentials [obtained by numerical diagonalization of the Hamiltonian (5)] relative to E_0/h, as a function of the interatomic distance R. The lowest potential has a minimum around $R \approx 0.8$ μm,

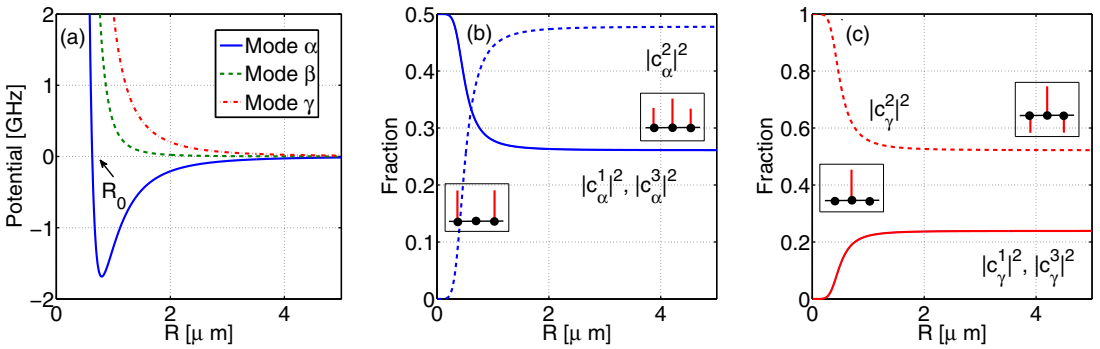

FIG. 2. (Color online) (a) The three collective potentials, U_k, as a function of the interatomic distance R. (b, c) The site populations $|c_k^i|^2$ as a function of the interatomic distance R in (b) the first ($k = \alpha$) and (c) the third ($k = \gamma$) collective states. The insets include schematically the site amplitudes at the three $|\pi_i\rangle$ states for the first and the third collective modes at large distances, $R > R_0$, and small distances, $R < R_0$.

which leads to a bound state of the atoms. In Figs. 2(b) and 2(c) we plot the fraction of each $|\pi_i\rangle$ state in the three collective states, with ($k = \alpha,\beta,\gamma$), that is, $|c_k^i|^2$, as a function of R. In mode α, for small distances the excitation is concentrated in the $|\pi_1\rangle$ and $|\pi_3\rangle$ states and the state $|\pi_2\rangle$ is almost not excited. For large distances, a collective state is obtained with half the excitation fraction in the $|\pi_2\rangle$ state and a quarter in each of the $|\pi_1\rangle$ and $|\pi_3\rangle$ states. In mode β (not shown) the $|\pi_2\rangle$ state is never involved in the formation of the collective state. In mode γ for small R the excitation is almost entirely localized in the $|\pi_2\rangle$ state, the $|\pi_1\rangle$ and $|\pi_3\rangle$ states are not excited. For large R the γ state has the same population distribution as the α state. The amplitudes of the three $|\pi_i\rangle$ states are plotted schematically in the insets of Figs. 2(b) and 2(c) for large and small R.

The situation is different when excitons are formed via dipole-dipole interactions involving ultracold ground and low-excited states in an optical lattice [28–30] or Rydberg states at larger separations than considered here [19,20]. Then the vdW shifts discussed above are usually negligible.

III. DYNAMIC RYDBERG AGGREGATE

After having established the effect of vdW interactions on the static properties of the exciton states in a chain of Rydberg atoms at fixed positions, we now consider dynamic properties of such a chain: a flexible Rydberg aggregate [21]. This is done by augmenting the total Hamiltonian of the problem with its kinetic energy part,

$$\hat{H}_{\rm kin} = \sum_i \frac{P_i^2}{2M}, \tag{7}$$

where P_i is the momentum of the ith atom and M is its mass (for the examples shown, we chose Li). The combined treatment of exciton dynamics and atomic motion is involved quantum mechanically, but can be treated very well using Tully's quantum-classical description [10,19,20,31]. In Tully's method, the internal electronic degrees of freedom are treated quantum mechanically, while the external position degrees of freedom of the atom are treated classically. The ith atom experiences the force

$$F_k^i = -\nabla_{R_i} U_k(\mathbf{R}), \tag{8}$$

according to one specific Born-Oppenheimer surface U_k. This surface corresponds to the kth eigenvector of the electronic Hamiltonian $H_{\rm ex}$. Due to these forces we obtain time-dependent atomic trajectories $R_i(t)$ from the equation of motion

$$M\frac{d^2R_i}{dt^2} = F_k^i, \tag{9}$$

and we obtain excitation amplitudes $c_k^i(t)$ from

$$i\partial_t|\Psi_k(t)\rangle = \hat{H}_{\rm ex}(\mathbf{R}(t))|\Psi_k(t)\rangle, \tag{10}$$

where $|\Psi_k(t)\rangle = \sum_i c_k^i(t)|\pi_i\rangle$. Stochastic nonadiabatic switches of the Born-Oppenheimer surface k are possible [31], but occur in a negligible fraction (<1%) of trajectories for all cases shown in the present paper. In our calculations we assume zero temperature. Actual experiments would be performed at ultracold temperatures, where on the time scales of interest thermal motion can be ignored; thus our zero temperature description is reasonable.

We consider one-dimensionally confined Rydberg aggregates. First, we discuss a trimer aggregate (i.e., three atoms), where we focus on the potential surface which stems from the combination of a repulsive vdW interaction and an attractive "pure dipole-dipole surface," as in the $k = \alpha$ state of Fig. 2(a), since this may allow a stable configuration due to the potential minimum.

For a symmetric trimer the forces on the atoms can be found analytically (in the Appendix we give detailed derivations of the symmetric aggregate); in the general case the corresponding energy landscape has the shape shown in Fig. 3, by using the Jacobi coordinates $r = R_2 - R_1$ and $R = R_3 - R_2 - r/2$. It allows stable bound trimer-aggregates in the global minimum around $r \approx 0.8\ \mu$m and $R \approx 1.2\ \mu$m, as seen from the magenta trajectory. Such a state can be created in a similar fashion as described in Ref. [20]. In this scheme first ground-state atoms are trapped in the desired arrangement, e.g., by using microlense arrays [32,33]. Then by laser excitation all atoms are transferred into the s state. Finally a microwave pulse that is short on the time scale of atomic motion addresses the desired aggregate eigenstate.

The binding on the lowest Born-Oppenheimer surface can be extended to larger aggregates, as shown in Fig. 4 for the

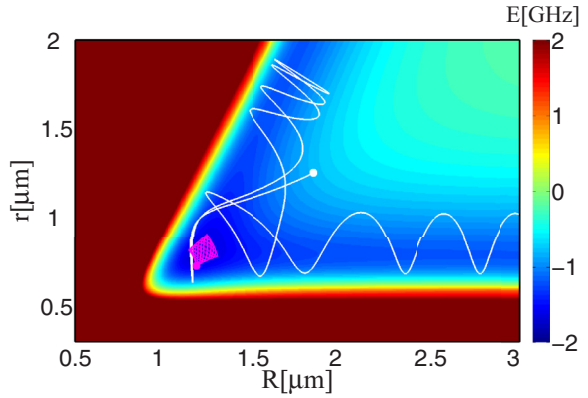

FIG. 3. (Color online) Energy landscape of the lowest Born-Oppenheimer surface of the Rydberg trimer. For ease of interpretation we use the Jacobi coordinates $r = R_2 - R_1$ and $R = R_3 - R_2 + r/2$. The potential exhibits a well around $R - r/2 \approx r \approx 0.8$ μm and exceeds the maximum of the color bar in the region of small r or R. Lines show a dissociating (white) and a stable (magenta) quantum classical trajectory. Big dots mark the starting position.

case of six atoms. The atomic initial position and momentum are randomly distributed, according to the quantum ground state of an initially harmonically confined particle, with spatial width $\sigma = 0.03$ μm. We then bin the atomic positions $R_i(t)$ to obtain the total atomic density $n(x,t)$. It shows partial dissociation, but a signature of the six-atom aggregate clearly remains visible. This stabilization crucially requires the modification of exciton states by the vdW shifts discussed earlier. Without them, the exciton wave function has insufficient amplitude on the outermost atoms and the attraction of these atoms becomes too weak. We choose a Rydberg state $n = 30$ to maximize the product of self-trapping frequencies in the aggregate and system lifetime (3 μs for the case shown). This empirically favors smaller principal quantum numbers.

Besides stable configuration one can prepare the system initially in configurations that exhibit a more complicated dynamics, e.g., the white trajectory shown in Fig. 3. Details for this trajectory are displayed in Figs. 5(a) and 5(b). We can access regimes in which the trimer first undergoes breathing oscillations with excitation transfer between the sites, only to finally dissociate into a dimer and a free atom at a dissociation time $t_{\rm diss} \approx 1$ μs, significantly faster than the excited system lifetime of about $\tau_{\rm life} = 6$ μs [18].

The dissociation can also be studied in a trajectory average, where we obtain the pictures shown in Figs. 5(c)–5(e). Here, we consider a chain which is slightly perturbed from a symmetric configuration. The position of each atom

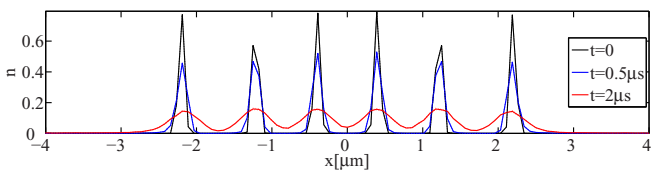

FIG. 4. (Color online) Total atom density n (arb. units) in vdW–stabilized Rydberg 6-mer for three selected times.

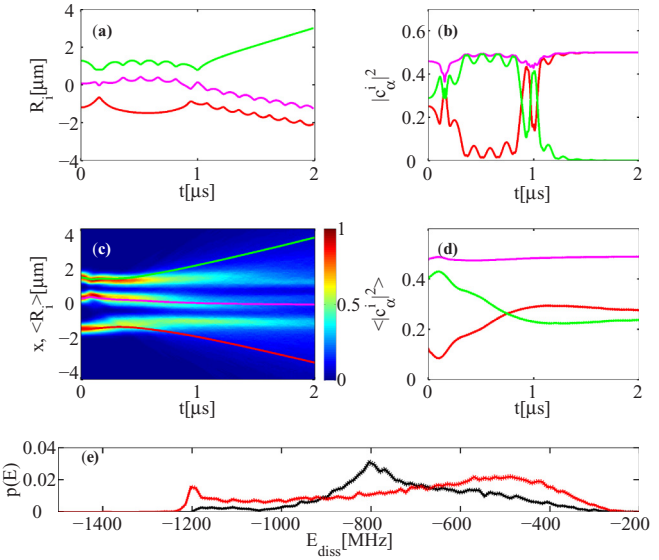

FIG. 5. (Color online) Rydberg aggregate dissociation for (a, b) symmetric and (c, d) asymmetric configurations. (a) Atomic positions R_i for a single dissociating trajectory, $i = 1$ [red (bottom) curve], $i = 2$ [magenta (middle) curve], and $i = 3$ [green (top) curve]. (b) Excitation amplitudes $|c^i_\alpha(t)|^2$ for a single dissociating trajectory. (c) Total atomic density n from the trajectory average; overlaid are the mean positions of the three atoms. (d) Mean excitation amplitudes $\overline{|c^i_\alpha(t)|^2}$ on the three sites. (e) Energy distribution of the final-state dimer (black solid curve) and the initial energy (red solid curve) for the same case in panel (c). The dotted lines indicate one standard error and are nearly indistinguishable from the solid ones.

is initially Gaussian-distributed around $x = -1.5$, 0.3, and 1.5 μm, with spatial widths of $\sigma = 0.2$ μm. In the dynamics we can resolve some coherent motion of the chain in the total atomic density [Fig. 5(c)], accompanied by excitation redistribution [Fig. 5(d)]. Later dissociation events that are qualitatively like those in Figs. 5(a) and 5(b) smear out the picture. Details of dissociation events depend strongly on the precise classical initial state, so that the multitrajectory simulation shows a quite broad distribution of the final dimer energy [34]. The smallest dimer potential energy is $U_{\rm min} \approx -1.2$ GHz and the largest initial total energy is about $U_{0,\rm tot} \approx -200$ MHz, explaining the bounds of the energy spectrum in Fig. 5(e).

The potential energy surface in Fig. 3 is reminiscent of that of simple triatomic molecules such as ozone for constrained bond angles. Modern theoretical methods can determine nuclear wave packets of such molecules during dissociation in detail [35], while only coarse grained quantities such as absorption spectra can be compared with experiments. One-dimensional confinement of Rydberg atoms may soon be possible optically [36,37], hence our system provides a platform for the direct experimental visualization of wave-packet dynamics in an analog of molecular-dissociation processes, with the use of state-selective and high-resolution Rydberg atom monitoring schemes [38–41]. Thus our setup allows the direct comparison of wave-packet evolution between theory and experiment.

IV. SUMMARY

In conclusion, we addressed the formation of excitons in chains of Rydberg atoms with short separations, where the vdW effect is shown to modify the excitonic picture formed by resonant dipole-dipole interactions. The level of excitation localization depends on the separation of atoms in the chain. We show that the combined action of vdW and resonant dipole-dipole forces can lead to interesting effects in one-dimensional chains, such as the stabilization of larger Rydberg aggregates in an attractive exciton. Even unstable parameter regimes show intriguing breakup dynamics that can be followed experimentally in quite some detail in the realm of ultracold Rydberg physics. Moreover, using the highest occupied molecular orbital and lowest unoccupied molecular orbital configurations, similar exciton-state modifications are expected for a cluster of organic molecules.

APPENDIX: SYMMETRIC RYDBERG AGGREGATE

For purpose of illustration, in this appendix we present detailed results for the case of a symmetric chain, where we can obtain instructive analytical results. In particular we focus on the case of three atoms. Then, due to the symmetry, we have $R_2 - R_1 = R_3 - R_2 \equiv R$.

To make the discussion more transparent, we approximate the electronic Hamiltonian by including interactions only among nearest-neighbor atoms; hence we obtain the following from Eq. (5) in the main text,

$$H_{\rm ex} = E_0 + \begin{pmatrix} D & J & 0 \\ J & \bar{D} & J \\ 0 & J & D \end{pmatrix}, \tag{A1}$$

where

$$J = \frac{hC_3}{R^3}, \quad D = \frac{h\left(C_6^{sp} + C_6^{ss}\right)}{R^6}, \quad \bar{D} = \frac{2hC_6^{sp}}{R^6}. \tag{A2}$$

Note that the energy difference between $|\pi_2\rangle$ and either one of the two states $|\pi_1\rangle$ and $|\pi_3\rangle$ is $\bar{D} - D$. Hence it depends on the difference between the C_6 parameters, that is, $C_6^{sp} - C_6^{ss}$.

The diagonalization of the Hamiltonian (A1) (for fixed atomic positions) gives the three eigenenergies U_k and the corresponding eigenstates $|\psi_k\rangle = \sum_{i=1}^{3} c_k^i |\pi_i\rangle$, with ($k = \alpha, \beta, \gamma$).

The eigenenergies are $U_\gamma = E_0 + D$ and

$$U_{\alpha,\beta} = E_0 + \frac{(\bar{D} + D)}{2} \mp \frac{1}{2}\sqrt{(\bar{D} - D)^2 + 8J^2}, \tag{A3}$$

where α corresponds to the $-$ sign and β to the $+$ sign, respectively. Using the same values for the parameters as in the main article, where $C_3 \approx -1.16$ GHz/μm^3, $C_6^{sp} \approx +282$ MHz/μm^6, and $C_6^{ss} \approx +47$ MHz/μm^6, we have verified that the resulting adiabatic potential surfaces are in very good agreement with the full numerical ones.

We also obtain analytical results for the site populations $|c_k^i|$, which are given by

$$\left|c_k^1\right|^2 = \left|c_k^3\right|^2 = \frac{J^2}{\Delta_k^2 + 2J^2}, \quad \left|c_k^2\right|^2 = \frac{\Delta_k^2}{\Delta_k^2 + 2J^2}, \tag{A4}$$

where $\Delta_k = U_k - D$, and we have $\sum_i |c_k^i|^2 = 1$. Note that the $|\pi_1\rangle$ and $|\pi_3\rangle$ states have identical site populations.

For the three collective electronic states $|\psi_k\rangle$, the atoms experience the above potentials $U_k(R)$ and move under the influence of the forces $F_k = -\nabla U_k(R)$. The calculation yields

$$F_{\alpha,\beta} = -\frac{(\bar{D}_R + D_R)}{2} \pm \frac{(\bar{D} - D)(\bar{D}_R - D_R) + 8JJ_R}{2\sqrt{(\bar{D} - D)^2 + 8J^2}}, \tag{A5}$$

with $\alpha \to (+)$, $\beta \to (-)$, and $F_\gamma = -D_R$, where

$$J_R = \frac{dJ}{dR} = -3\frac{hC_3}{R^4},$$
$$D_R = \frac{dD}{dR} = -6\frac{h\left(C_6^{sp} + C_6^{ss}\right)}{R^7}, \tag{A6}$$
$$\bar{D}_R = \frac{d\bar{D}}{dR} = -12\frac{hC_6^{sp}}{R^7}.$$

The trajectories of the interatomic distances are the solutions of the equations $\frac{M}{2}\frac{d^2R}{dt^2} = F_k$.

We numerically solve the equations of motion to get the trajectories for different initial interatomic distances. The initial velocity is taken to be zero and the mass of the atom is that of Li, $M \approx 11.1 \times 10^{-27}$ Kg. In Fig. 6(a) the system is prepared in the lowest symmetric state for different initial interatomic distances. When the initial interatomic distance is smaller than the crossover length, the potential is repulsive and

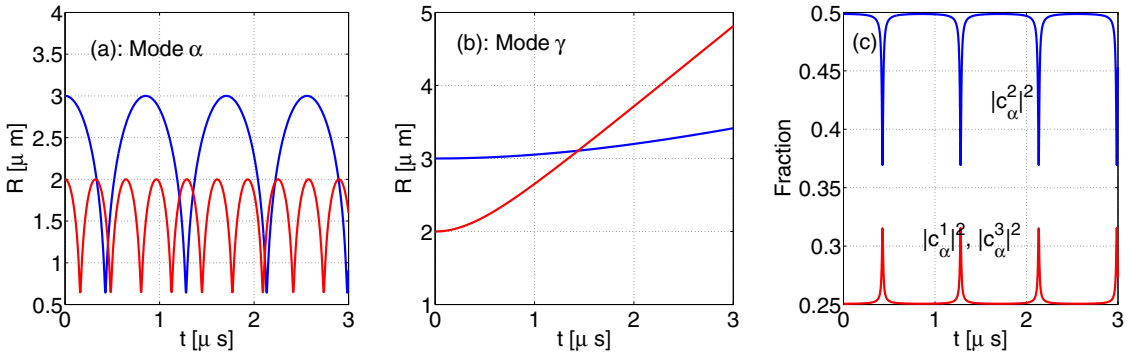

FIG. 6. (Color online) (a) The interatomic distance trajectories for the lowest symmetric eigenstate. (b) The trajectories for the higher eigenstate. The plots are for different initial interatomic distances of 2 and 3 μm. (c) The populations $|c_k^i|^2$ in the lowest mode as a function of time for initial interatomic distance of 3 μm. The trajectory oscillations result in population oscillations with a period of about 0.85 μs.

the atoms move apart. When the starting distance is larger than the crossover length, the potential is initially attractive and the atoms oscillate around the minimum of the potential. For the upper collective state the trajectories are plotted in Fig. 6(b) for different initial interatomic distances. Here the potential is repulsive and the interatomic distances increase with time. Interestingly, the oscillations of the trajectories around the minimum of the potential in the lowest symmetric state lead to oscillations in the populations of each $|\pi_i\rangle$ state in the global exciton state as is presented in Fig. 6(c).

[1] J. Frenkel, Z. Phys. A **59**, 198 (1930).
[2] J. Frenkel, Phys. Rev. **37**, 17 (1931).
[3] S. Davydov, *Theory of Molecular Excitons* (Plenum, New York, 1971).
[4] V. M. Agranovich, *Excitations in Organic Solids* (Oxford University Press, Oxford, 2009).
[5] H. Zoubi and G. C. La Rocca, Phys. Rev. B **71**, 235316 (2005).
[6] J. Roden, A. Eisfeld, M. Dvořák, O. Bünermann, and F. Stienkemeier, J. Chem. Phys. **134**, 054907 (2011).
[7] M. Müller, A. Paulheim, C. Marquardt, and M. Sokolowski, J. Chem. Phys. **138**, 064703 (2013).
[8] M. Müller, A. Paulheim, A. Eisfeld, and M. Sokolowski, J. Chem. Phys. **139**, 044302 (2013).
[9] F. Robicheaux, J. V. Hernández, T. Topçu, and L. D. Noordam, Phys. Rev. A **70**, 042703 (2004).
[10] C. Ates, A. Eisfeld, and J. M. Rost, New J. Phys. **10**, 045030 (2008).
[11] M. Saffman, T. G. Walker, and K. Molmer, Rev. Mod. Phys. **82**, 2313 (2010).
[12] T. F. Gallagher and P. Pillet, Adv. At. Mol. Opt. Phys. **56**, 161 (2008).
[13] S. Bettelli, D. Maxwell, T. Fernholz, C. S. Adams, I. Lesanovsky, and C. Ates, Phys. Rev. A **88**, 043436 (2013).
[14] M. Kiffner, H. Park, W. Li, and T. F. Gallagher, Phys. Rev. A **86**, 031401(R) (2012).
[15] M. Kiffner, W. Li, and D. Jaksch, Phys. Rev. Lett. **110**, 170402 (2013).
[16] M. Kiffner, W. Li, and T. F. Gallagher, J. Phys. B: At. Mol. Opt. Phys. **46**, 134008 (2013).
[17] M. Kiffner, W. Li, and D. Jaksch, Phys. Rev. Lett. **111**, 233003 (2013).
[18] I. I. Beterov, I. I. Ryabtsev, D. B. Tretyakov, and V. M. Entin, Phys. Rev. A **79**, 052504 (2009).
[19] S. Wüster, C. Ates, A. Eisfeld, and J. M. Rost, Phys. Rev. Lett. **105**, 053004 (2010).
[20] S. Möbius, S. Wüster, C. Ates, A. Eisfeld, and J. M. Rost, J. Phys. B: At. Mol. Opt. Phys. **44**, 184011 (2011).
[21] K. Leonhardt, S. Wüster, and J. Rost, arXiv:1310.6975.
[22] T. Pohl and P. R. Berman, Phys. Rev. Lett. **102**, 013004 (2009).
[23] H. Park, P. J. Tanner, B. J. Claessens, E. S. Shuman, and T. F. Gallagher, Phys. Rev. A **84**, 022704 (2011).
[24] H. Park, E. S. Shuman, and T. F. Gallagher, Phys. Rev. A **84**, 052708 (2011).
[25] K. Singer, J. Stanojevic, M. Weidemüller, and R. Côté, J. Phys. B: At. Mol. Opt. Phys. **38**, S295 (2005).
[26] E. Altiere, D. P. Fahey, M. W. Noel, R. J. Smith, and T. J. Carroll, Phys. Rev. A **84**, 053431 (2011).
[27] J. Nipper, J. B. Balewski, A. T. Krupp, B. Butscher, R. Löw, and T. Pfau, Phys. Rev. Lett. **108**, 113001 (2012).
[28] H. Zoubi and H. Ritsch, Phys. Rev. A **76**, 013817 (2007).
[29] H. Zoubi and H. Ritsch, Europhys. Lett. **90**, 23001 (2010).
[30] H. Zoubi and H. Ritsch, Adv. At. Mol. Opt. Phys. **62**, 171 (2013).
[31] J. C. Tully, J. Chem. Phys. **93**, 1061 (1990).
[32] G. Birkl, F. B. J. Buchkremer, R. Dumke, and W. Ertmer, Opt. Commun. **191**, 67 (2001).
[33] F. Nogrette, H. Labuhn, S. Ravets, D. Barredo, L. Béguin, A. Vernier, T. Lahaye, and A. Browaeys, arXiv:1402.5329.
[34] We wait for the classical trajectory to have clearly dissociated and then determine the kinetic plus potential energy of the dimer part of the system only.
[35] N. Balakrishnan and G. D. Billing, J. Chem. Phys. **101**, 2968 (1994).
[36] L. Li, Y. O. Dudin, and A. Kuzmich, Nature London **498**, 466 (2013).
[37] R. Mukherjee, J. Millen, R. Nath, M. P. A. Jones, and T. Pohl, J. Phys. B: At. Mol. Opt. Phys. **33**, 184010 (2011).
[38] A. Schwarzkopf, R. E. Sapiro, and G. Raithel, Phys. Rev. Lett. **107**, 103001 (2011).
[39] B. Olmos, W. Li, S. Hofferberth, and I. Lesanovsky, Phys. Rev. A **84**, 041607(R) (2011).
[40] G. Günter, M. Robert-de-Saint-Vincent, H. Schempp, C. S. Hofmann, S. Whitlock, and M. Weidemüller, Phys. Rev. Lett. **108**, 013002 (2012).
[41] G. Günter, H. Schempp, M. R. de Saint-Vincent, V. Gavryusev, S. Helmrich, C. S. Hofmann, S. Whitlock, and M. Weidemüller, Science **342**, 954 (2013).